University of Aveiro Physics Department,
2018

Nazar
Romanyshyn

Estudo e desenvolvimento do sistema inovador para leitura e aquisição de dados em PET

Study and development of an innovative readout system for PET scanners.

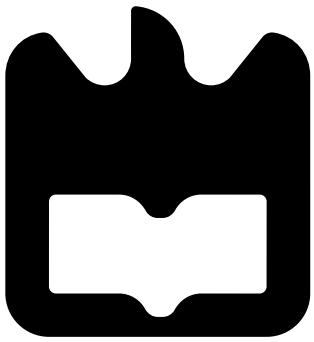

University of Aveiro Physics Department,
2018

Nazar
Romanyshyn

Estudo e desenvolvimento do sistema inovador para leitura e aquisição de dados em PET

Study and development of an innovative readout system for PET scanners.

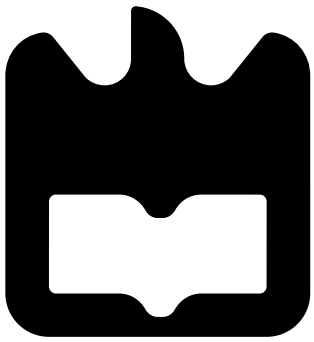

Nazar
Romanyshyn

Estudo e desenvolvimento do sistema inovador para leitura e aquisição de dados em PET

Study and development of an innovative readout system for PET scanners.

Tese apresentada à Universidade de Aveiro para cumprimento dos requisitos necessários à obtenção do grau de Mestre em Engenharia Física, realizada sob a orientação científica do Doutor João Filipe Calapez de Albuquerque Veloso, professor associado c/ agregação do Departamento de Física da Universidade de Aveiro e do Doutor Pedro Manuel Mendes Correia.

o júri / the jury

presidente / president

Professora Doutora Margarida Maria Resende Vieira Facão

Professora Auxiliar, Departamento de Física, Universidade de Aveiro

vogais / examiners committee

Professor Doutor Fernando Domingues Amaro

Professor Auxiliar Convidado, Departamento de Física, Faculdade de Ciências e Tecnologia, Universidade de Coimbra

Professor Doutor João Filipe Calapez de Albuquerque Veloso

Orientador, Professor Associado C/ Agregação, Departamento de Física, Universidade de Aveiro

agradecimentos

Queria agradecer aos meus pais que me sempre apoiam ao longo da minha vida, ao professor João Veloso e ao Pedro Correia que me ajudavam ao longo do meu mestrado, ao todo o grupo de investigação DRIM da Universidade de Aveiro que eu conheci durante este tempo... sobretudo a Ana Luisa, o Carlos Azevedo e a Lara Filipa. Por fim quero agradecer aos meus colegas de curso que estiveram comigo durante esses cinco anos, obrigado pelo vosso apoio, suporte e pelas boas memórias.

acknowledgements

I would like to thank my parents who have always supported me throughout my life, to Professor João Veloso and to Pedro Correia who helped me throughout my master's degree, to the entire DRIM research group at the University of Aveiro that I met during this time. .. especially Ana Luisa, Carlos Azevedo and Lara Filipa. Finally, I want to thank my classmates who were with me during these five years, thank you for your support and good memories.

Resumo

No final desta tese, foram estudadas várias cadeias resistivas com aplicação no scanner easyPET. Para cada uma delas foi encontrada a tensão operacional ótima. Foi também possível desenvolver o algoritmo que é capaz de encontrar e selecionar os dados descartando energias fora da região dos picos de 511 keV, de modo a melhorar a separação entre os picos sem variar a largura total do histograma. Concluímos que é possível reduzir o número de canais eletrónicos necessários para o registo de dados, o que simplifica o sistema eletrónico e reduz o seu custo total.

Abstract

In the end of this thesis, several resistive chains with application in easyPET scanner were successfuly developed. It was found the optimal operational voltage for each one of them. It was possible to develop the algorithm that is capable to find and to select the data by discarding energies outside the 511 keV peak region, so the separation between the peaks becomes better without varying the total width of the histogram. We concluded that it is possible to reduce the number of required electronic channels for recording data, that makes the electronic system simpler and reduces its total cost.

Contents

List of Figures

List of Tables

.

Chapter 1

Essential physics of Positron Emission Tomography (PET)

1.1 Radioactive decay law and β^+ decay

Radioactive decay is the process of transformation in which the unstable atom (radioisotope) emits the excess of the particles (electron, positron, neutrino) and (or) energy (photon) until it reaches a stable state. The relation between the radioactive and stable atoms is known as the radioactive decay law which is given by an eq.(1.1)

$$N(t) = N(0)e^{-\lambda t} \tag{1.1}$$

where t defines the time, $N(t)$ is the number of radioactive nuclides at the instant t, $N(0)$ defines the initial number of radioisotopes and λ is the decay constant. By using this law, we can derive two basic concepts that are used for the work with the radionuclides: the half-life time and the activity [5, 6].

The half-life time $t_{0.5}$ defines the time that is needed for the radioactive source to decrease the number of parent nucleus by a half. By solving the equation (1.1) as $N(t_{0.5}) = \frac{1}{2}N(0)$ we get that $t_{0.5} = \ln(2)\lambda^{-1}$. Another important concept that is used is **the activity** A, this is by definition the derivative of N in order of t $A = \frac{dN}{dt}$ where N is also given by eq.(1.1). The activity's SI unit is known as Bequerel (Bq), in a honor of a person who discovered the natural radioactivity in 1896 Mr. Henri Bequerel. The half-life time and the activity are very important because they allow us to choose the radionuclide that usually don't last longer than

the PET acquisition, and also that are safe for the biological tissues [5, 7].

From all possible radioactive decays, PET imaging uses positron (β^+) emitting radionuclides. **The positron** is the antiparticle of the electron, that has the same mass (9.11×10^{-31} kg) but the opposite charge (1.6×10^{-19} C). In positron (β^+ decay) the radioemitting nuclide has one more proton p, which is converted into a neutron n. The resulting daughter nucleus C gains one neutron and loses one proton. To obey the conservation of mass and charge, there are also the emission of (β^+) particle, neutrino ν.This decay is represented by an eq.(1.2).

$$ {}^{n+p}_{p}B \rightarrow {}^{a+b}_{b}C + \beta^+ + \nu \tag{1.2} $$

where B defines the decayed radionuclide (daughter nucleus), $a = n + 1$, $b = p - 1$, ν defines the neutrino. In this decay, p is converted into a n and into a β^+ that is emitted from the nucleus with the ν. The neutrino is a particle that is not detected, however its emission guarantees the conservation of mass[1, 9].

1.2 Interactions of the particles with the matter

When we define the interactions between the particles and the matter, we generally speak about the interactions between the particle (charged or radiation) and the electron of one of the atomic shells. However, there is still a probability of some interaction between the particle and the nucleus.

1.2.1 Interactions of the charged particles

When a particle passes near the nucleus, it may be affected by its electric field, since the nucleus consists of protons and neutrons. So when when it happens, the positron is scattered from its path and emits part of its kinetic energy in the form of X-ray radiation. This is also known as *Bremsstrahlung* radiation [7].

As the positron is released to the medium that is full of the electrons, it starts to interact with them due to the opposite charges which is known as the Coulomb interaction. As the result, the β^+ particle is scattered from its initial trajectory and transfers a part of its energy to the electrons of the environment, so the respective atom becomes excited. As the positron will keep interacting with the electrons it will keep losing its kinetic energy [6].

After transferring most of its kinetic energy the positron recombines with one of the electrons in the process known as annihilation. In this process, the mass of positron and electron

is converted to the energy which is released in the form of two γ-ray photons, each one with 511 keV and in the opposite direction (1eV=1.6×10^{-19}J). The interaction of the positron and its annihilation are represented at the figure1.1. The line that represents the emission of two photons is called Line of Response (LOR).

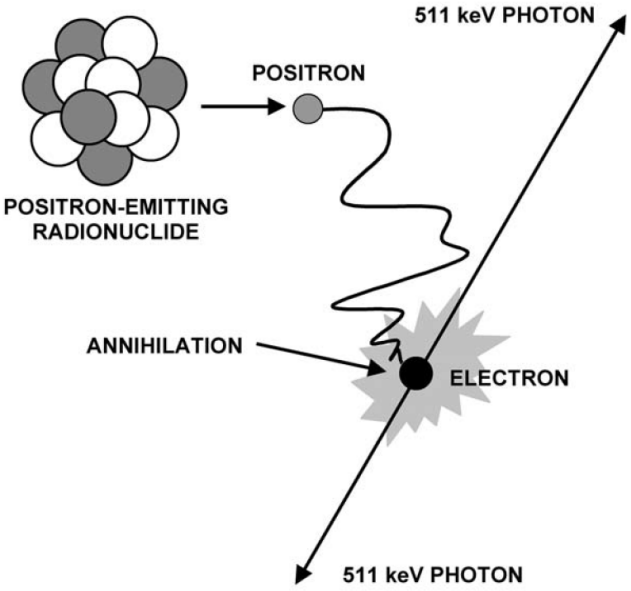

Figure 1.1: Annihilation of a positron-emitting radionuclide [3].

The range of the positron particle depends on its kinetic energy and the density of the absorbing medium. The higher kinetic energy means that the β^+ moves with higher velocity and has more energy to transfer, which is why it has a bigger range. It is important to pay attention to the range of the emitted particle because it defines the lowest spatial resolution of the obtained image. If the particles range will be big when is compared to the dimension of the object, then it is not possible to estimate a location of an emitting radionuclide. If its range is small, then it would be much easier to detect the true location of the β^+ emitting radionuclide. The table 1.1 shows a few examples.

The first three radionuclides (^{11}C,^{13}N,^{15}O) given at the table 1.1 have been widely used in PET imaging due to the high positron percentage decay. The abundance of their stable atoms in the biological compounds, makes those radionuclides easy to work with. Their presence in the synthesized molecule does not significantly alter its properties, and they can be easily produced. Their disadvantage is their low half-life time, which makes them useful to study only short physiological processes [1].

Table 1.1: Some of the β^+ emitting radionuclides in PET imaging. Adapted from [5, 11, 12].

Nuclide	Half-life	Decay mode (%)	$E_{\beta^+,max}$ (MeV)	R_{mean}(mm)
^{11}C	20.4 min	β^+ (99.8)	0.960	1.2
^{13}N	9.96 min	β^+ (100)	1.190	1.8
^{15}O	2.03 min	β^+ (99.9)	1.720	3.0
^{18}F	109.6 min	β^+ (97)	0.635	0.6
^{22}Na	2.6 years	β^+ (90)	0.540	0.6
^{68}Ga	67.71 min	β^+ (89.14)	0.830	1.9
^{124}I	4.18 days	β^+ (25)	2.140	0.8

The ^{18}F is the most used radionuclide in PET imaging. It is synthesized by the bombardment of the ^{18}O atoms with the the highly energized protons p, that is accelerated by a cyclotron. This reaction is given by eq.(1.3), where n defines the neutron [1, 13].

$$^{18}\mathrm{O} + p \rightarrow ^{18}\mathrm{F} + n \tag{1.3}$$

^{124}I is a PET radiotracer that can be used for the diagnosis and treatment of differential tyroid cancer, hepatocellular carcinoma (HCC) and to study longer physiological processes. When comparing ^{124}I PET imaging with the conventional gamma scintigraphy, the results obtained for ^{124}I show more accurate measurements of metabolic tumor volumes. However, there are still studies that must be made to improove a dosimetry protocols [14, 15].

The last to mention ^{22}Na radionuclide, due to its long half-life time is used for the calibration purposes.

1.2.2 Interactions of the γ-rays with the matter

The γ-ray photon has no charge. While interacting with the environment particles, there are two possible ways they can transfer their energy: they can transfer it all at once and disappear (Photoelectric effect), or they can transfer it by colliding with many particles (Rayleigh or Compton Scattering) and being scattered in every interaction [6].

The predominance three main types of interactions (compton scattering, pair production and photoelectric effect) are illustrated at the figure 1.2 in terms of the atomic number and of the photons energy.

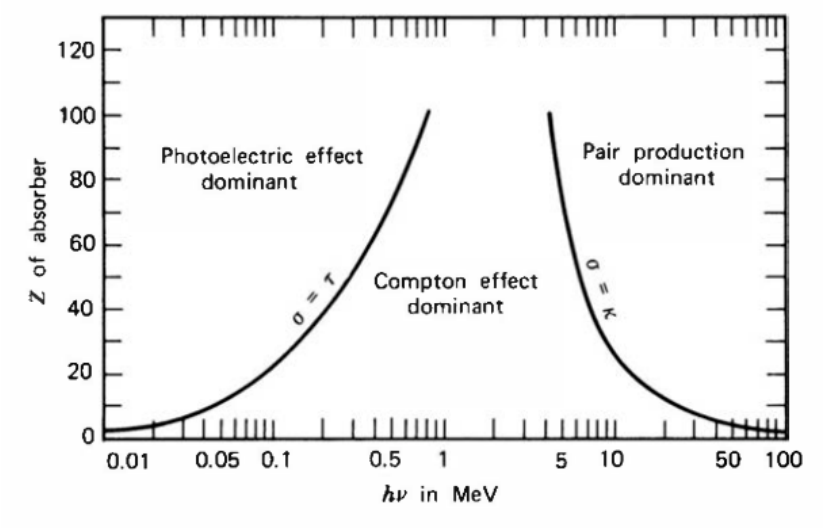

Figure 1.2: The predominant interaction between the particle of energy (hν) and the matter of atomic number (Z), the image taken from [5].

This figure is divided in three regions where each region has the predominant type of interaction, that depends on the atomic number Z and the photons energy $h\nu$. The lines between the regions define the atomic number Z and the energy of the photon for which both of interactions have the same probability of occurrence.

Photoelectric effect

In this interaction, the γ-ray photon transfers all its energy to an electron from one of the atomic inner energy levels and causes the removal of the electron. The resulting kinetic energy of the ejected photo-electron is given by eq.(1.4)

$$E_C = h\nu - W \tag{1.4}$$

where $h\nu$ defines the energy of the photon, and W defines the binding energy of an electron from its atomic shell. As a result, the ejected electron leaves a vacancy which makes the atom positively charged. This state is quickly occupied by an electron from a higher energy level. That electron also leaves the unoccupied state which later becomes occupied by an electron from a higher energy state. When the electron transits from the higher to the lower energy state it emits the excess of energy as a photon. This process of rearrangement occurs until all of the states will be again occupied [2].

Compton scattering

In a Compton scattering, the γ-ray photon transfers a part of its energy to the electron that is bounded to the nucleus of an absorbing atom. As a result, the electron is ejected from the atom, the photon is scattered and its remaining energy (E_{sc}) is given by an eq.(1.5), where E_0 defines the energy of the photon before the collision. This type of scattering is exemplified at the figure 1.3.

$$E_{sc}(\text{keV}) = \frac{E_o}{1 + \frac{E_o}{511} \times \left(1 - \cos(\theta)\right)} \tag{1.5}$$

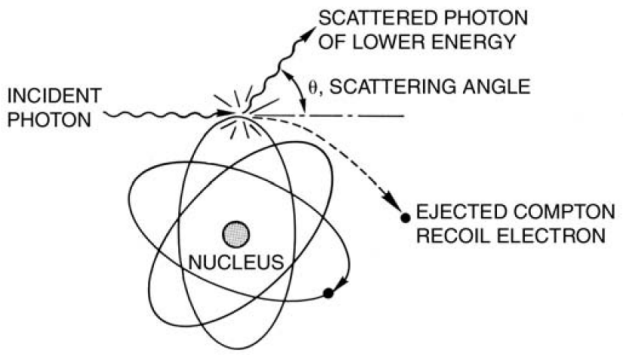

Figure 1.3: The ilustration of Compton effect. Image taken from [3].

According to the conservation of the energy, the kinetic energy of the ejected electron (E_{kin}) may be given by the eq.(1.6)

$$E_{kin} = E_0 - E_{sc} - W \tag{1.6}$$

where W defines the binding energy of the electron to the nucleus of the absorbing atom.

Rayleigh scattering

After the collision with an electron, the γ-ray photon is slightly scattered from its initial direction by an angle dθ and its energy after collision is approximately equal to its energy before the collision. Because there is no significant transfer of energy, this type of interaction is considered as elastic collision. As the result, the γ-ray photon just gets scattered from its initial trajectory [6].

Pair production

Pair production occurs when the γ-ray photon of 1.022 MeV collides with the nucleus of the atom. As a result, the photon transforms into two particles, the electron and the positron. Each one has the kinetic energy of 0.511 MeV that combined conserve the total moment of the incident 1.022 MeV γ-ray photon. Eventually, the emitted positron will annihilate and yields two γ-ray photons each with the energy of 0.511 MeV [6, 7].

At this chapter we have seen the possible interactions between the primary and secondary products of the radioactive decay and the matter, we have also understood the relation between the energy, atomic number and the predominant interaction of radiation particle and the matter. With this information we understand the processes of the emission of radiation and its interaction. Now we can start to describe the principles of PET imaging.

.

Chapter 2

Positron Emission Tomography (PET)

Positron Emission Tomography is the most sensitive non-invasive imaging technique that was developed for the use in a field of nuclear medicine and has been used as one of the most important imaging tools since the 1990s. It provides the medical physician with a information about the metabolic activity of the object of study (say it is a laboratory animal such as a mouse or a rat, or a patient). Based on the given information, the expert can detect the presence of anomalies, diseases, even in its early studies of the development [1, 2, 13, 16].

In this technique, the radio-emitting substance is injected into the object of study and is tracked down by the detectors in a unique way(the detection in coincidence). The detected information is then used for the volumetric-image reconstruction. By analyzing the reconstructed image and based on the type of an injected substance, it is possible to study the brain activity, the glucose distribution, the heart functioning and to estimate the location of cancer cells inside of the body [1, 2, 12].

2.1 The key principles of PET

The tracer principle was discovered in the early 1900s by Mr. George de Hevesy. According to principle, once injected into the object, the radioactive compounds have the same behavior in the physiological processes of the object as its own substances. Mr. Hevesy prooved that this is true by studying the behavior of the substance made of salt and the radioactive isotope of lead once it has been absorbed by a plant. By measuring the radioactivity along the different parts of a plant, he concluded that his substance accumulated more in the roots rather than in the leaves [2].

In the case of PET imaging, this principle is essential to estimate the location of a radiotracer in the object of study. As the cancer cells consume more glucose compared to other cells of the organism, the experts use the substance made of the radio-emitting nuclide and a molecule which is similar to glucose. Once the resulting substance is injected into a patient, it is consumed more by the tumor cells and tends to accumulate at their region. Consequently, these areas have an increased amount of radioactivity when compared with other areas of the patient section [2]. The most commonly used substance for this purpose is [^{18}F]-FDG (fluorodeoxyglucose) which is described in the next section.

The tomography principle allows visualizing the inside part of the object without any surgery intrusion. It translates from the Greek as tomos-"slice" grapho-"drawing". Unlike a projection image, that converts a 2D image of a volumetric object by compressing the information of the object along one of three dimensions, the tomography represents the 3D object by giving 2D slices along the third dimension [2].

2.2 Radiotracer

Nowadays it is possible to synthesize many (β^+) emitting substances whose behavior is similar to the bio-substances. This enables to use them in PET imaging to study many different metabolism processes of the body.

The most common use of fluorine ^{18}F, is with the molecule fluordeoxyglucose (FDG). The fluorine must be attached (labelled) to the molecule known as 2-deoxy-D-glucose. Together they form a radiotracer known as The resulting compound is more known as [^{18}F]-FDG (fluordeoxyglucose). Its molecular structure is shown in the figure (2.1). This radiotracer behaves in the body as glucose molecule and its accumulation in the cells occurs at the same rate as glucose. This enables to use it for the study of glucose activity in the organism. Based on this information, it is possible to study the brain activity, as well as to detect the anormal acumulation of the glucose in the body. This approach is practiced for the pre-diagnosis of brain diseases (such as Parkinson or Alzeimer), or for the treatment of the tumor cells. [^{18}F]-FDG was found to be usefull mostly in the fields of the oncology, cardiology and neurology [13].

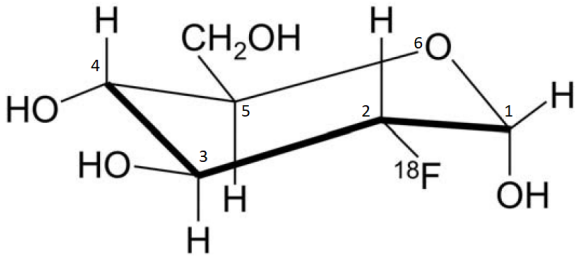

Figure 2.1: The molecular structure of [^{18}F]-FDG image taken from [1].

2.3 The data aquisition and image reconstruction

When the radionuclide is introduced into the object of study, this substance is distributed inside of the object according to the tracer principle. The emitted γ-ray photons are normally detected by a thick ring of detectors that surrounds the object. These detectors are connected to the electronic system that enables to detect the pair of photons that were emitted from the same annihilation. The detection of both photons must occur in the time interval of a few nanoseconds, this techniques is known as coincidence detection. The figure (2.2) represents an example of the detection of two photons in the coincidence. The line that links two detectors is the Line of Response (LOR). The collected data contains, the coordinates (x, y, ϕ) that help to redraw each of the detected LORs. The coordinates (x,y) give a minimum distance from the reference point up to the LOR, when the angle ϕ helps to define its inclination on the 2D plane.By representing all of the detected LORs we obtain a 2D cross sectional image of an object for a certain coordinate z and by representing all of the 2D planes we obtain the volumetric image of the object. Based on this image, the expert concludes if there is some issue in the metabolic activity of the object.

2.4 Why do we need to develop PET for small animals?

When we talk about the studies at small animals, we mean laboratory mice and rats. First and foremost its because these animals have many diseases that are encountered in humans. In this way, it is possible to study the behavior of the disease in animals, so that then this knowledge could be used to produce the best drugs for humans. For this purpose it is necessary to develop the small PET scanners. The size of a small scanner is defined as one third or one fourth to the size of a typical scanner that is used in humans. When comparing the size of

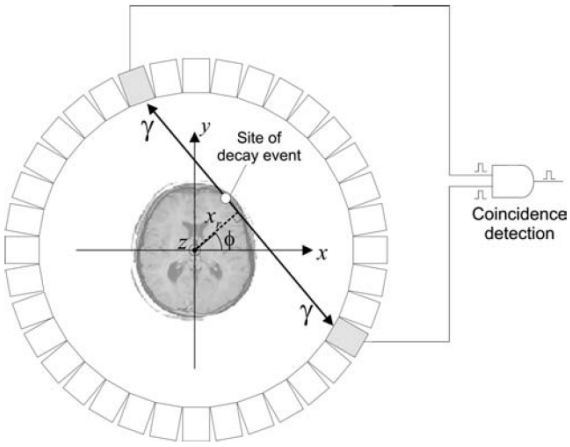

Figure 2.2: Schematic diagram of electronic collimation (coincidence detection) in PET. Image taken from [2].

detectors, in the case of man, the sensitive area reaches to 4-6 mm^2 [17], while in our laboratory detectors are used in 1-2 mm^2. The reason why it is necessary to reduce the entire system several times is due to the size of the object of study. It is so much smaller when compared to human that there is no ohter way but to use the detectors with better spatial resolution.

Before the advent of PET in the mid-90's, such types of analyzes were plagued by a huge amount of laboratory animals, because it was impossible to obtain information about food and drug concentration in the body without surgical intervention. PET provided the opportunity to collect this data without the need to sacrifice the laboratory animal. Thus the same animal can be used by researchers for more than one analyzes, which reduces the total number of animals needed for a study (which eventually will reduce the total cost). Normally taking care only of one laboratorial rat may cost up to the 1000$ [2]. Also, the ability to monitor the pharmacokinetics of a particular drug reduces the time spent on their development. The reasons mentioned above make PET an indispensable tool for studying animal diseases and for developing new prototypes. Despite these benefits, the necessary technology is still very expensive, its price ranges between 400,000$ and 1,200,000$ [18]. One can say that this is another obstacle to the development of this research sector. At the moment, one of the goals is the development of a cheaper PET scanner that would deliver a high quality images. One of these devices is produced in the Aveiro University by the DRIM group and the start-up company RI-TE, the name of the project is easyPET.

The easyPET concept

One of the first spotlights of the easyPET when comparing it to the other PET devices for small animal studies, is its detector system. It consists of two arrays of detectors that are mounted one in front of the other. The lack of detectors is compensated by the mounted motor system that synchronously spins around the object of study. Another difference that worth an attention is the electronic readout of the data. The conventional PET devices use one electronic channel per detector, so far the easyPET electronics uses two electronic channels per one array of detectors (which is 16 detectors per each array). With those two upgrades, it was possible to reduce the total cost about 10 times when comared to another PET system for preclinical studies. Hovewer, the reduced ammount of detectors makes easyPET less sensitive when compared with the others [17].

.

Chapter 3

Radiation detectors and signal processing

After the annihilation, the γ-ray photon interacts with the particles of the absorbing environment, after what its energy is absorbed in the detector and converted into electric pulse.

The energy of the γ-ray photon is absorbed and converted into photons of visible light in the material known as scintillator. The absorbed energy is divided and converted into many optical photons, which are detected by a photon detector. The output of the optical detector is the amplified electric pulse that was obtained due to the incident photons. This process of γ-ray detection and its convertion to the electric pulse of charge is ilustrated at the figure 3.1.

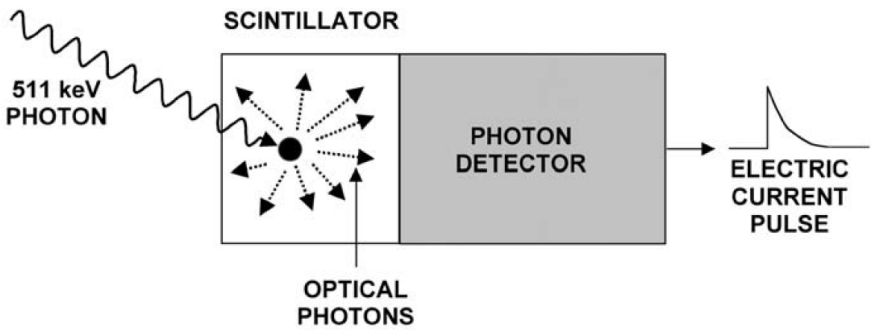

Figure 3.1: Simplified representation of γ-ray detector. Image taken from [3].

In the next sections I would like to explain a little bit more about the scintillator, photon detectors and processing circuit.

3.1 The scintillator

The scintillator is a material whose principle of operation is based on the phenomenon of luminescence. According to this principle, the energy transfered by the incident high energetic (such as ultra-violet, X-ray or γ-ray) particle is distributed and emitted in a form of photons of visivble light. In general, all scintillators can be divided into two groups: organic and inorganic. In our case, we will talk about inorganic scintillators, due to their high density which is needed to absorb the incident γ-ray photons. They may be described as crystalls that are transparent to the visible light, that are made of atoms with a large atomic number and have a small amount of impurities. These impurities represent other atoms that have a key role in the emission of visible light.

The process of generating visible light photons is divided into three stages: conversion, transport, and luminescence. In the first step, the γ-ray photon interacts and excites the electrons up to the conduction band, as long as the transfered energy to the electron is high enough to overcome the E_{gap} and to occupy one of the conduction band states. When they are excited, these electrons leave behind in the E_V band an unocuppied state also known as hole. In the stage of transport, the created charge carriers (electrons and holes) travel along the material to the lower energetic states, the traps that were added due to the dopants. Finally, the emission of visible light occurs with the recombination of the electron and hole. The presence of the traps allows the emission of energy in the region of visible light. The mentioned process of energy absorption and relaxation of the scintillating material is exemplified by using the energy diagram in the figure 3.2.

In the choice of a good scintillator, one must pay attention to its key parameters such as the stopping power, light yield, scintillation decay time and energy resolution. The stopping power is the parameter that defines the mean distance that γ-ray photon needs to go through the scintillator material to transfer all of its energy to this material. It is proportional to the atomic number of the material Z and the density of the scintillator ρ that by $\rho \times Z^{[3-4]}$. The higher stopping power also allows to reduce the volume of the scintillator [12, 19, 20, 21].

The light yield is the parameter that defines the number of optical photons that are emitted by material per absorbed unit of energy. Usually, the number of emitted photons is defined per 1 keV or per 1 MeV, the bigger light yield delivers bigger output signal and consequently

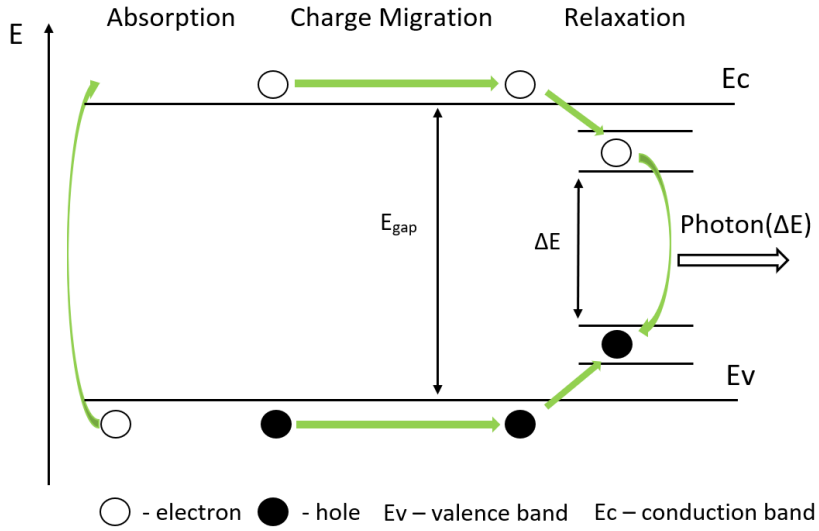

Figure 3.2: Smiplified representation of energy bands of inorganic scintillator.

the bigger *Signal to Noise Ratio* (SNR) [12, 22]. The emission of visible photons is not instantaneous and can take from a couple of nanoseconds up to a few milliseconds. The relation between the light output intensity and the time is shown at the figure (3.3).

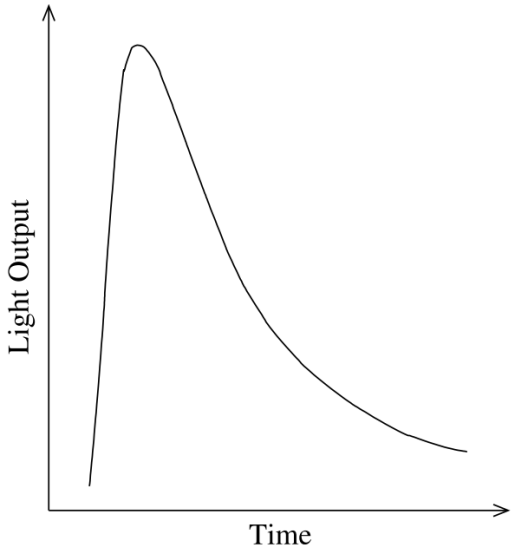

Figure 3.3: Time profile of scintillator, image taken from [9].

This pulse is given by an eq.(3.1), where L_0 defines the maximum value of the light emission curve, τ_r defines the rise time and τ_d defines the decay time. The decay time is the time difference given by t$(0,37L_0)$-t(L_0), and t$\geqslant$ t(L_0) [9].

It is important to pick the scintillator with the small decay time, to increase the accuracy of the γ-photon energy measurement.

$$L = L_0(e^{-t/\tau_d} - e^{-t/\tau_r}) \tag{3.1}$$

With this being said, the table (3.1) shows some of the inorganic scintillators that are currently used for PET imaging and studies. When compared with another scintillating materials, LYSO or LYSO:Ce is one of the best choices. For this purpose there were used arrays of LYSO:Ce crystals.

Table 3.1: Scintillator crystals and their characteristics [1, 6, 7, 8, 9, 10].

Scintillator	Density (g/cm^3)	Light Yield 10^3(Ph/MeV)	Scintillation time (ns)	Maximum emission λ_{max} (nm)	Energy resolution (0.511 MeV,%)	Hygroscopic
NaI:TI	3.67	38	230	410	10	Yes
CsI:TI	4.51	64	630	550	4.3	Yes
BGO	7.13	6	300	480	20	No
GSO:Ce	6.71	10	60	440	8.5	No
LSO	7.40	29	40	420	10	No
LYSO	7.1	30	40	375	7	No
LYSO:Ce	7.1	32	40	420	8	No
$LaBr_3$:Ce	5.3	61	35	358	8	Yes

3.2 The photodetector

Once the visible light photons have been generated, they must be converted into electrical current that could be processed by electric circuit and stored in the memory of the computer. Usually, a scintillator is coupled with a photodetector, that converts the incident photons into electrons and after multiplicates them in a specific way which outputs the current. There are two common photodetectors that are used in PET: photomultiplier tubes (PMTs) and solid-state photodetectors like avalanche photodiodes (APDs) [3].

3.2.1 Photomultiplier tube (PMT)

The photomultiplier tube is a photodetector that mainly consists of an entrance window and a series of dynodes that are located in vacuum. Once the light photon enters into the PMTs

entrance window, it's converted into a photo-electron with a probability of 15-20%. This means that for each 100 incident photons, only 15-20 of them can actually eject an electron. Each of the ejected electrons heads up to the first dynode due to the potential difference between the photocathode and the dynode. There, each one of them ejects more electrons and after all of them are accelerated to the second dynode due to the potential difference. After extracting more electrons on the second dynode, the electrons are accelerated up to the next dynode, where they release more electrons and so on. In the end, when the electric flux hits the anode, the output signal is sufficiently high to be processed by the electronic channel. Overall, the total gain of the PMT and its effects are related to the applied potential, the number of dynodes and its material is given by an eq.(3.2)

$$G = \alpha \times \delta^N \tag{3.2}$$

where α defines the fraction of emited photoelectrons that reaches the first dynode, δ defines the number of secondary electrons emitted per incident electron and N defines the number of dynodes in PMT [5].

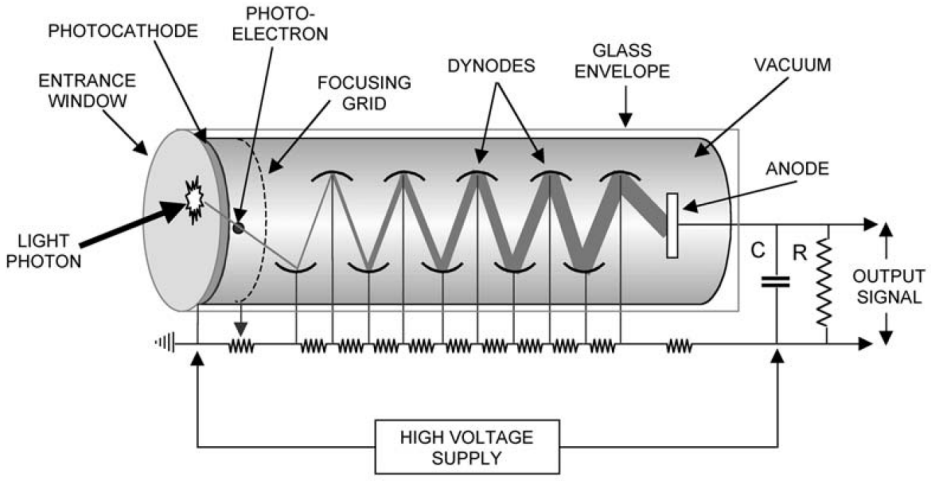

Figure 3.4: Representation of PMT and the detection of the photoelectron. Image taken from [3].

3.2.2 Solid state photodetectors

The avalanche multiplication

The avalanche multiplication is a process in which an incident light photon creates an electron-hole pair in one of the photodiode layers, which after causes a chain of electron-hole

ejections known as avalanche multiplication.

The first originated electron and hole are drifted by the high electric field up to the cathode and anode respectively. On their path through the semiconductor layers, they suffer many collisions with the atoms of those layers. As the result, the traveling charges (electron and hole) transfer to the atoms a part of their kinetic energy. If this energy happens to be higher than the bandgap of the respective semiconductor layer than the traveling charge can create another electron-hole pair. Eventually, the new created pair will behave in the same way as the first one. Due to the design of the avalanche photodiode, this process occurs numerous times before the electron and hole reach the cathode and anode respectively. By operating in determined conditions, the photodiode is able to detect a single light photon [23].

Avalanche photodiode (APD)

Avalanche photodiode is a solid state device that is capable, in its operating range wavelength, to detect a single photon. It consists of a pn junction that is sandwiched between two higly doped semiconductor layers p^{++} at the top and n^{++} at the bottom. The schematic representation of APD is given in the figure 3.5.

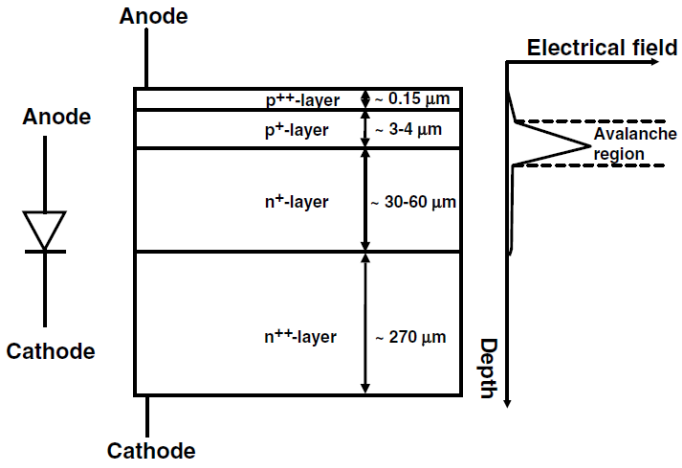

Figure 3.5: Representation of the layer structure in the APD and the intensity of an electric field along the depth. Image taken from [2].

Once APD operates in Geiger-Müller mode, its gain can reach up to the 10^6. In this mode, the aplied reversed voltage is higher than the breakdown voltage ($V_{op} \geqslant V_{br}$) and can be easily damanged by its own produced ammount of charge. To avoid such damage, each of

the APD's is connected in series with a quenching resistor (R_q) that drops the applied APD's voltage every time when the produced charge passes throug it. In this way, the applied voltage gets lower than the breakdown region and the avalanche stops growing. However, the active area of a single APD is extremely small, which is why a single used photodetector consists of a series of APD's+R_q that are connected in paralel. Such schematic is exemplified at the figure 3.9 (a). This type of solid photodetector is known as Multi Pixel Photon Counter (MPPC).

Multi Pixel Photon Counter (MPPC)

Multi-pixel photon counter (MPPC) defines the photodetector that consists of many pixels that are connected in parallel. Each pixel is defined as the APD that is connected in series with a quenching resistor. Those pixels altogether define what is known as the active region that detects the photons. Each photon produces the same amount of charge q, while the n detected photons, produce the charge Q that equals $n \times q$. The figure 3.9 (b) represents the incidence of a three photons and the respective discharged pulses. After the detection, the resulting pulse, which in this case has an amplitude given by $Q = 3 \times q$, enters the electronic channel where the pulse is processed and then stored in a database.

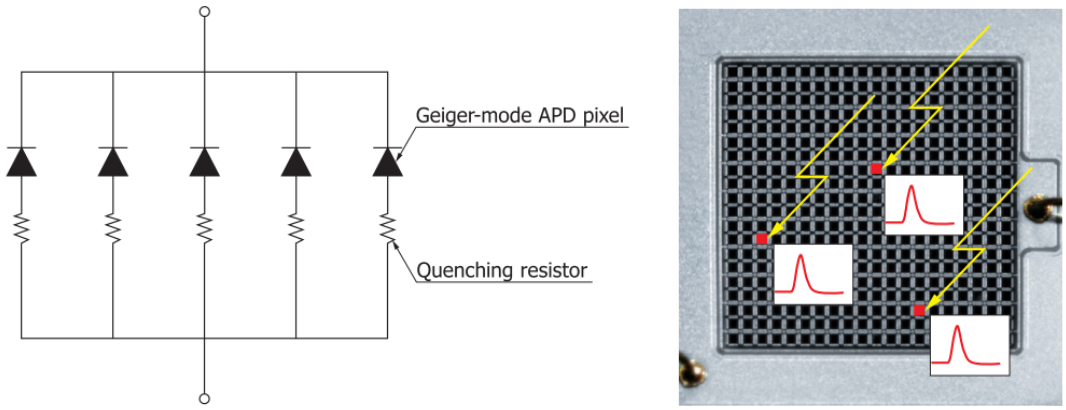

(a) (b)

Figure 3.6: Schematic representation of (a)- the APD's+R_q connected in paralel and (b)- the active area of MPPC. Images taken from [4].

3.3 Processing circuit

For being able to analyse the detected amount of charge, the pulse has to be processed by an electronic circuit that consists of several stages. There are three main stages in the pulse processing that can be resumed as the following: the pre-amplification, shaping, and discrimination. Only then the obtained data is stored and may be analyzed [5, 9]. The analog pulse that is discharged by a photomultiplier is not enough to be processed or counted by the electronics, which is why first it needs to be amplified. For this purpose, because of the scintillation time, the best choice would be to use an amplifier that integrates all charge outputed by a photodetector. Its basic circuit scheme is shown at the figure 3.7 as a charge sensitive preamplifier. The output of this stage is voltage pulse V that is proportional to the input charge pulse. Then the output V heads up to the shaping amplifier.

The shaping amplifier converts the input V pulse into a suitable processing pulse shape and filter it from the electric noise. It consists of three different blocks: high-pass filter, amplification, and a low-pass filter. At the high-pass filter eliminates the noise of low frequency and transforms the input signal into a pulse that is given by

$$V(t) = V \times e^{(-t/\tau)} \tag{3.3}$$

where τ is the time constant. It reduces the pulse overlapping (*pile-up*) and is useful especially when the pulse rate is high. Then, the pulse is amplified and finally, it passes through the low pass filter. This filter eliminates the noise of high frequency and also adapts the shape of the pulse so its height could be measured by the rest of the circuit [5, 9].

The discriminator is the stage, where the circuit selects all the input pulses that are above a pre-selected threshold or between upper and lower selected threshold values. After that, all of the selected pulses are converted in the digital form by Analog to Digital Converter ADC and sotred in the computer [5, 9].

3.4 The resistive chain

The resistive chain, is a number of resistors that are linked in series. Between every connection of two resistors, there is also connected an MPPC. This system is exemplified in figure 3.8.

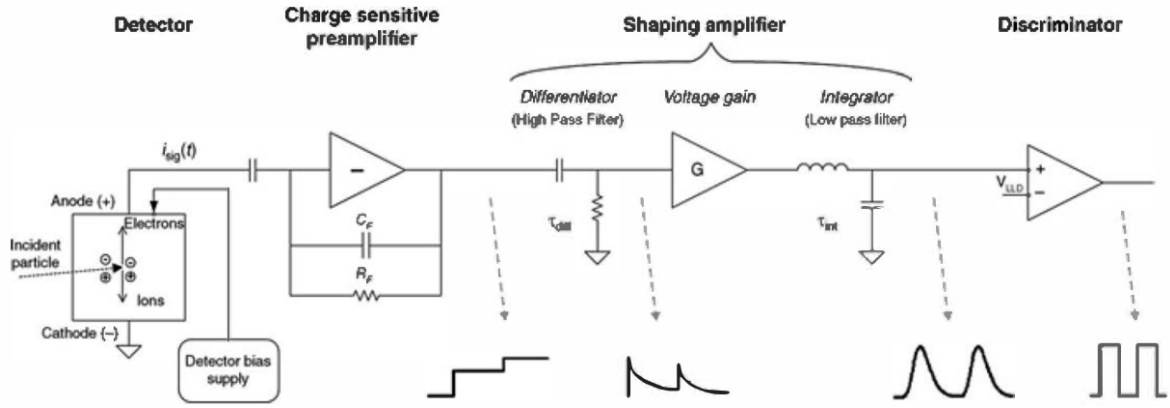

Figure 3.7: Exemplified scheme of processing circuit. Image taken from [5].

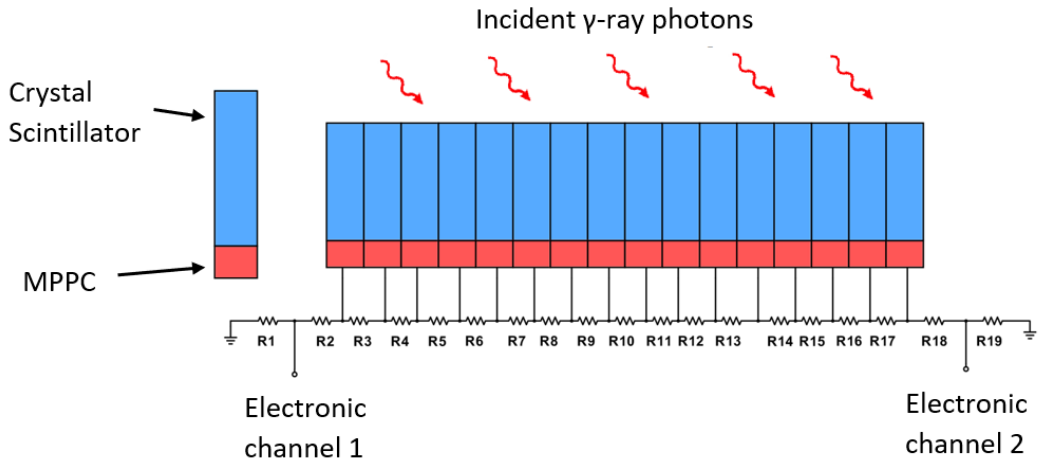

Figure 3.8: Exemplified resistive chain array of 16 MPPC's.

Instead of using one processing circuit, electronic channel, per each MPPC the resistive chain enables to use only two electronic channels $Ch_{1,2}$ to process the charge from a whole array of γ-ray detectors. Eventually, this upgrade reduces a lot the total complexity of the processing circuit, as well as its total cost. Once the pulse of charge enters the resistive chain, it is divided into two smaller pulses. Each one of them heads along the resistive chain into different directions up to the respective channel $Ch_{1,2}$. Then the signal is processed and stored in the computer. To find out which of the MPPC's has been discharged the pulse into the chain, we have to determine the normalized ratio between two recorded pulses which is given by the eq.(3.4)

$$Ratio = \frac{Ch_1 - Ch_2}{Ch_1 + Ch_2} \tag{3.4}$$

where $Ch_{1,2}$ define the amplitude of the pulses that were recorded in each channel. The sum

of the channels $Ch_1 + Ch_2$ contains the information about the energy of the detected photon and from here, we can get another information about the energy of the detected particles. The amplitude that is digitalized by an electronic channel is proportional to the energy of γ-ray particle that was transferred to the γ-ray detector.

3.5 Detectors that were used and their experimental setup

Initially, the idea was to mount all arrays with γ-ray detectors at the laboratory. However, their assembly had to be made with high control and quality. After trying different approaches and due to the high standards that were required for the soldering of resistive chains with the MPPC's arrays, this idea was abandoned. All of them were assembled at the company specialized in the electronic soldering. The figure 3.9 represents the final products of the MPPCs arrays that were studied. The array, called array nº1, shown at the figure 3.9 (a) uses 16 MPPC's of a serie S10362-11-100P with the resistive chain of 17 resistors each of 5 Ω (with tolerance of 5%). The array nº2 has 16 MPPC's of a series S13360-1350P with the resistive chain of 17 resistors each one of 5 Ω . The array, called array nº3, shown at the figure 3.9 (b) shows the array of the 40 MPPC's of a serie S13615 with the resistive chain of 41 resistors of 5 Ω (with tolerance of 5%), it is important to mention that the figure represents only a half of this resisive chain. It's another half was soldered on the other side of PCB (Printed Circuit Board). [24, 25, 26].

The figure (3.10 (a)) represents the mounted detectors and the ^{22}Na β^+ emittting source, while on the figure (b) it is represented the processing board, so called U-shape board that was designed for the signal processing of γ-ray pair photons in coincidence. The experimental setup consisted of the γ-ray detectors (scintillator crystals coupled with the MPPC's), the resistive chain for a readout of the amplified charge by MPPC's. For the processing of the data, it was used the U-shape board that was already developed. To prevent the intervention of the external light, during the data acquisition the detectors were placed inside of a black box and were irradiated with a not-collimated γ-ray source. Two of the three wires that are connected to each of the array detectors connect them with two electronic channels and the third one is used to polarize the MPPC's.

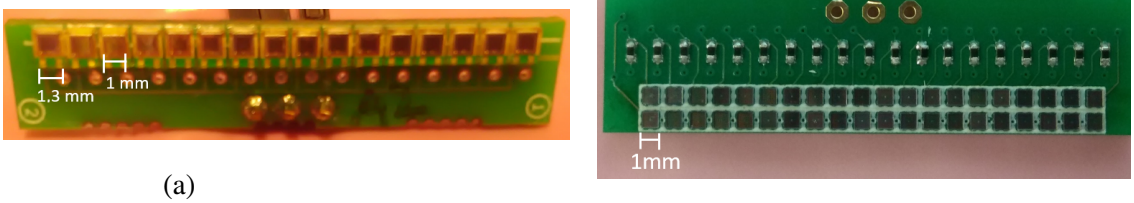

(a) (b)

Figure 3.9: (a) - Detector array nº1; $R_{eq} = 85\Omega$; (b) - Detector array nº3; $R_{eq} = 205\Omega$.

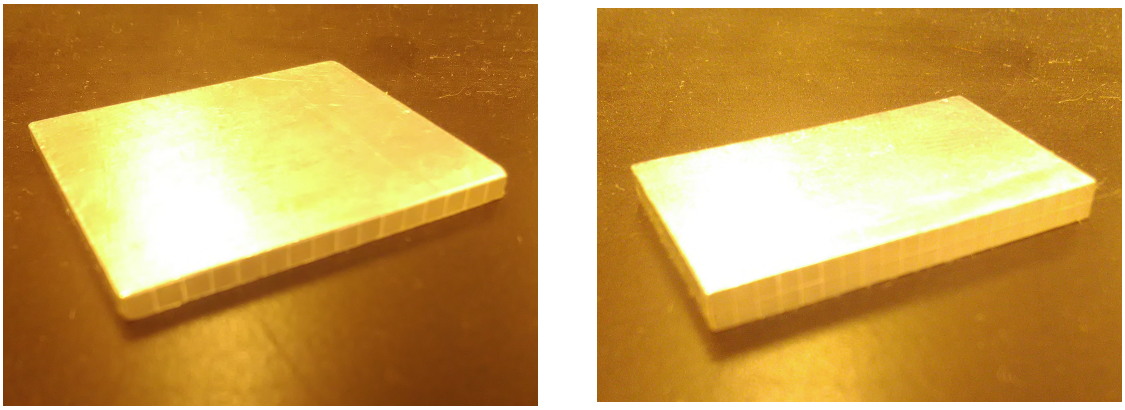

(a) LYSO array of 16 crystals each one of 2x2x30mm.

(b) LYSO array of 40 crystals each one of 1.5x1.5x20mm.

Figure 3.10: Crystal scintillators used for data aquisitions.

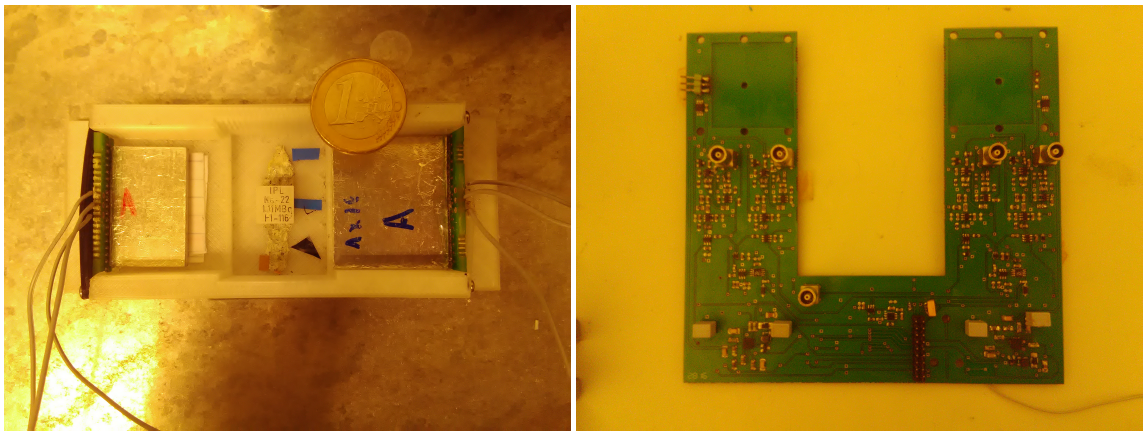

(a) (b)

Figure 3.11: On the left (a) is represented a γ-ray detector setup, while on the right (b) is represented the board that was designed for processing the signals.

.

Chapter 4

Representation and analysis of the obtained results

The aim of those experiments was, based on the ratio and energy resolution, to find out the optimal voltage operation parameter for each one of the used detector arrays. Each one of the detectors arrays was irradiated by the ^{22}Na source with the activity of 1.1 MBq and the acquisition time of 20 minutes.

The acquired data was used to represent the ratio spectrum. Then, the detected data was identified respectively for each of the detectors. This data was used for the Gaussian interpolation and finally, based on the fitted curves, according to the eq. (4.2) and (4.3) there were obtained the values of ratio resolution. The energy resolution was obtained based on the data that was collected by each one of the used detectors. For each of them, it was represented the respective energy spectrum where the detected 511 keV photons were fitted up to the Gauss curve. Then, by using the interpolated standard deviation parameter, the energy resolution was obtained according to the eq. (4.2) and (4.4).

$$G(x) = A \times e^{-(x-H)^2/(2\times\sigma^2)} \tag{4.1}$$

$$\sigma \simeq 2.35 \times \mathrm{FWHM} \tag{4.2}$$

$$\mathrm{R_{Ratio}}(\%) = \frac{\mathrm{FWHM}}{2} \times 100 \tag{4.3}$$

$$R_{Energy}(\%) = \frac{FWHM}{H} \times 100 \tag{4.4}$$

There, the 'A' defines the amplitude of the pulse, 'H' defines the center of the peak, σ defines the standard deviation of the curve and FWHM defines the full width at the half maximum of the curve. From there, the interpolated functions were used to determine the ratio resolution given by eq. (4.3). The treatment of the obtained data was done using MATLAB® software, version 2018b. The obtained values, for each of the three studied arrays are represented in the next three sections.

Table 4.1: The best obtained values for the studied detectors.

Detector array nº	Ratio resolution (%)	Energy resolution(%)	Operational voltage (V)
1	1.15±0.3	17.5±2	74
2	1.5±1	15±5	57.5
3	1.39±1.1	18.1±15	57

4.1 Resolution studies with the detector array nº1

From the V_{op}=74.3 V, the discharged pulses start to saturate and the ratio resolution begins to increase. From the studied operational voltages for this array, the optimal operational voltage is 74 V. The energy resolution of the detectors while they operate at 75.9 V, gets out of control. In this case, it is impossible to quantify the energy of the particles and, consequently it gets impossible to draw the lines of the response. The most probable explanation for this result is that the MPPC detector starts to create the avalanches of such magnitude that due to the inner charge interactions, the true information just gets corrupted.

The blue triangles point up to the peak coordinates, each of the peaks contains the the γ-ray photons that were detected by the detectors. The red curves are the Gaussian interpolations, given by an eq. (4.1), that were obtained for each one of the detected peaks. From there, the interpolated functions were used to determine the ratio resolution given by using an eq. (4.2) and (4.3).

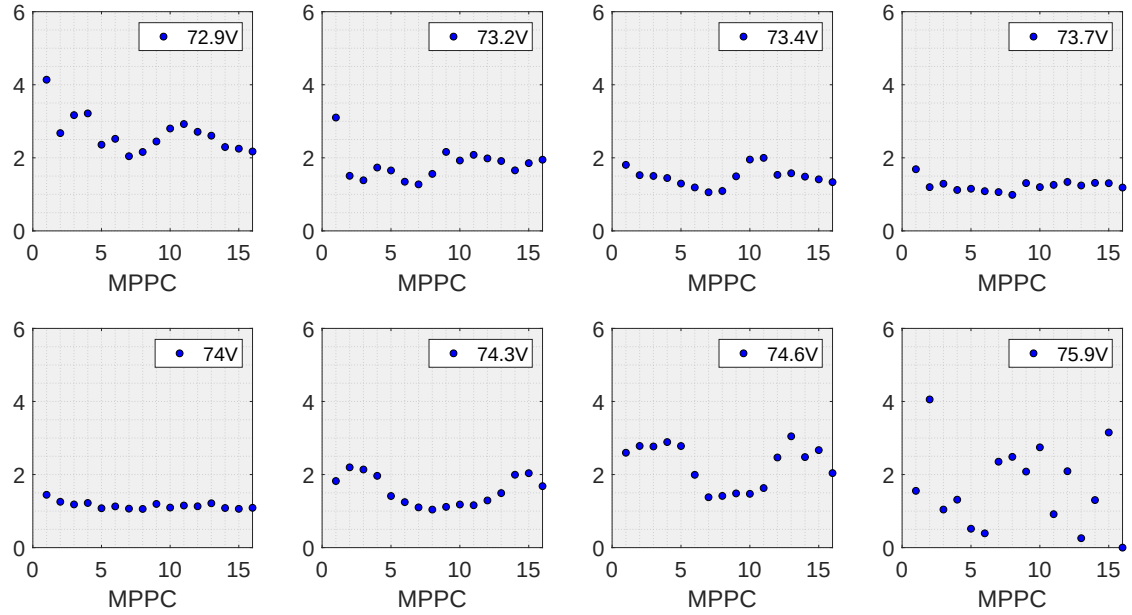

Figure 4.1: Ratio resolution(%) for a resistive chain of 80 Ω obtained for 16 MPPC's+LYSO defined at the figures ((3.9) and 3.10 (a)) respectively.

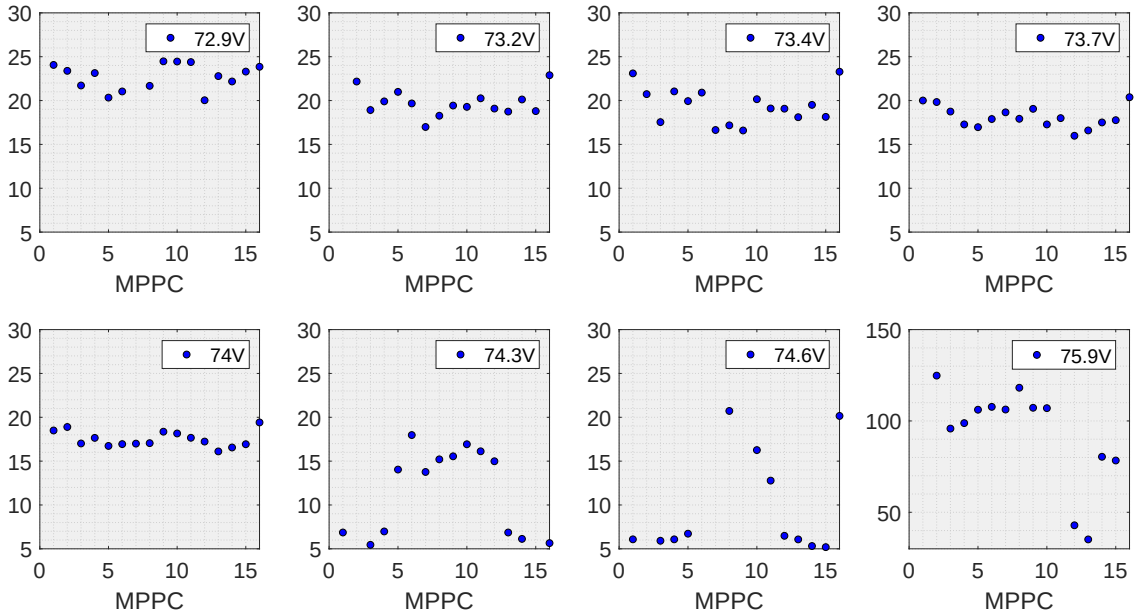

Figure 4.2: Energy resolution(%) for a resistive chain of 80 Ω obtained for 16 MPPC's+LYSO defined at the figures ((3.9) and 3.10 (a)) respectively.

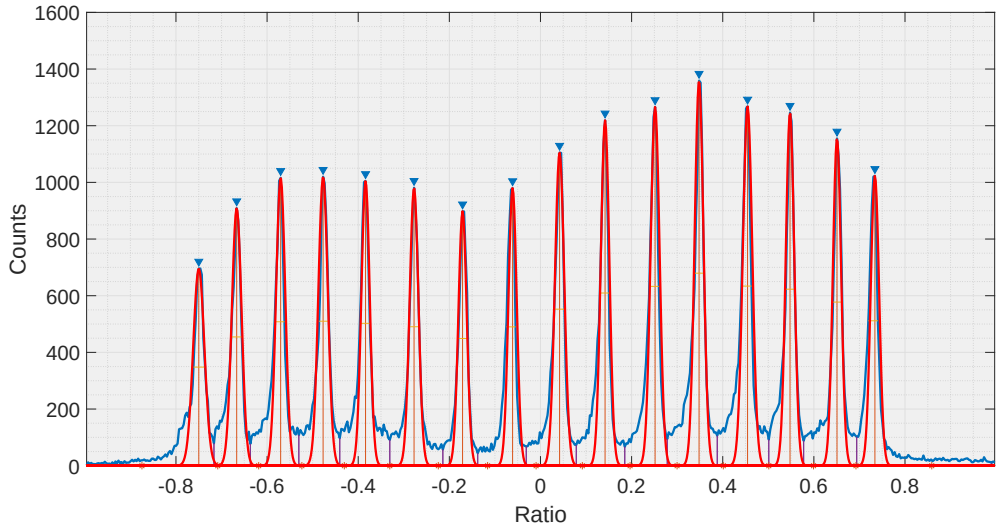

Figure 4.3: The obtained ratio spectrum for the detectors array with V_{op}=74 V.

The difference in counts observed in the peaks of ratio spectra at the figure 4.3 may be due to different optical coupling between scintillators and MPPCs along the array. This zone of contact, between the scintillator and the MPPC, is critical for the transfer of photons. There there is always a probability of the light loss. Consequently, this will reduce the total number of avalanches and the total number of the counts.

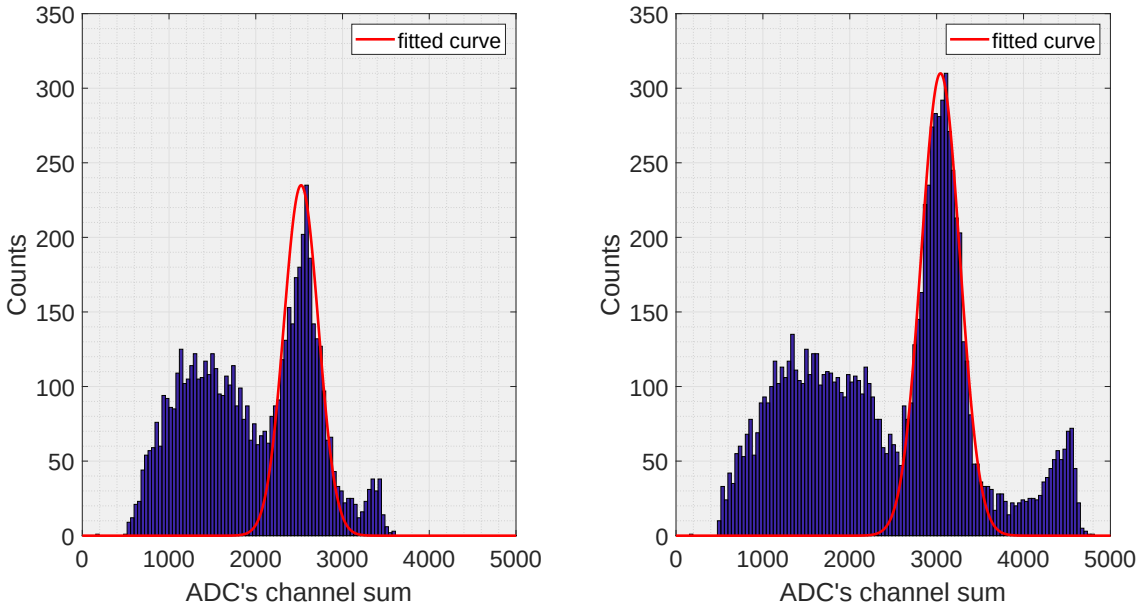

Figure 4.4: Energy spectrums detected by two detectors. The respective ratio peaks (1^{st} and 12^{th}) are represented at the figure (4.3).

Another possible reason for the light loss is due to the misalignment between the scintillator and MPPC. It may be that the active region of the MPPC is partially out of the contact with the scintillator. In this way, the misaligned MPPC would never detect all the photons that transferred from the scintillator. When compared this case with the ideally aligned detector (MPPC+LYSO) where the unique difference is the detector alignment, the second one will have more counts that the first one, just because it receives more photons from the scintillator. For the same V_{op} of 73.4 V, the figure 4.4 represents the energy spectrum of the two detectors, with the best (peak nº12) and the worst (peak nº 1) energy resolution respectively.

The curve tend to fit up to the caracteristic peak that represent the number of γ-ray photons which energy is around 511 keV. These are the detected γ-ray photons that didn't interact with the matter or their interaction were negligible, a.e. Rayleigh scattering. For the case of the ^{22}Na this peak represents the true events that were detected and that can be used to estimate the location of the β^+ radioisotope. The values on the left of the fitted peak define the particles that somehow interacted with the matter and were scattered, due to the Compton effect.

4.2 Resolution studies of the detector array nº2

By using the same ^{22}Na positron-emitting source, the same type of study was made for a different array of detectors (V_{br} $\approx$54 V). The obtained values of resolution are shown at the figures 4.5 and 4.6. The optimal operational voltage parameter obtained for this detector array is of 57.5 V. The respective ratio spectrum is shown at the figure 4.7.

As it can be seen at the figure 4.7, the given ratio spectrum in the middle of the spectrum there is data that was detected by the two detectors. The more probable reason for this is due to misalignment between the MPPC's and the scintillator LYSO array. If we compare the figures 4.3 and 4.7, it is possible to notice that at the figure 4.3 the distance between the peaks is uniform while at the figure 4.7 this distance changes along the spectrum.

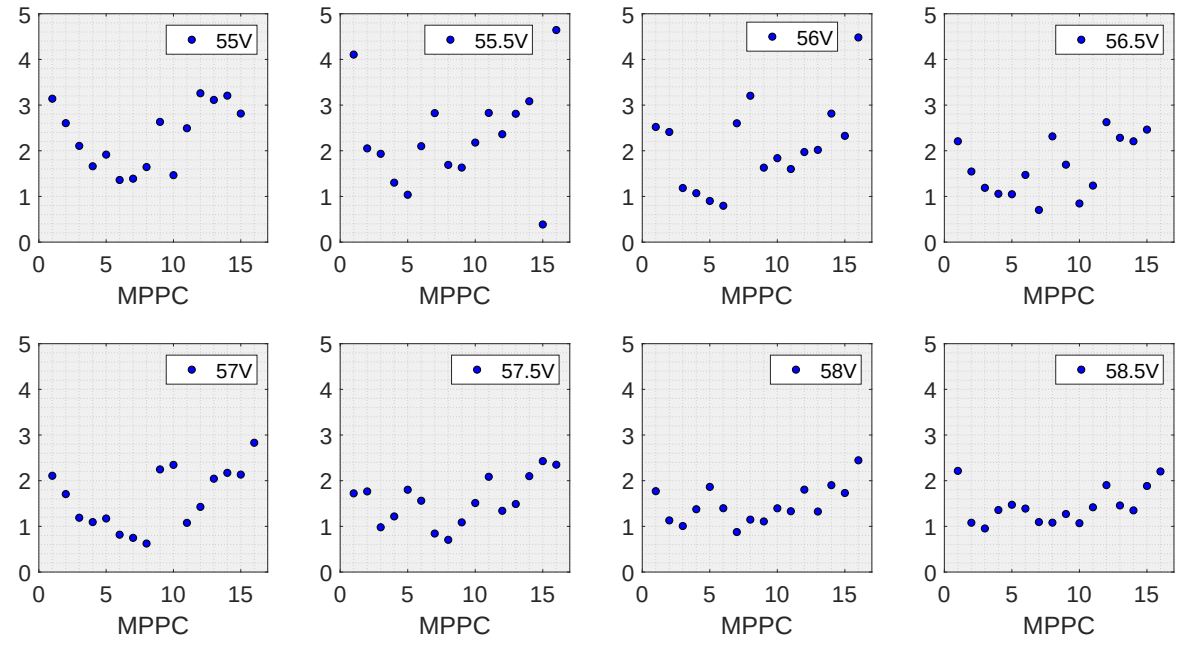

Figure 4.5: Ratio resolution(%) for a resistive chain of 80 Ω obtained for 16 MPPC's+LYSO. The LYSO array is defined at the figure 3.10 (a).

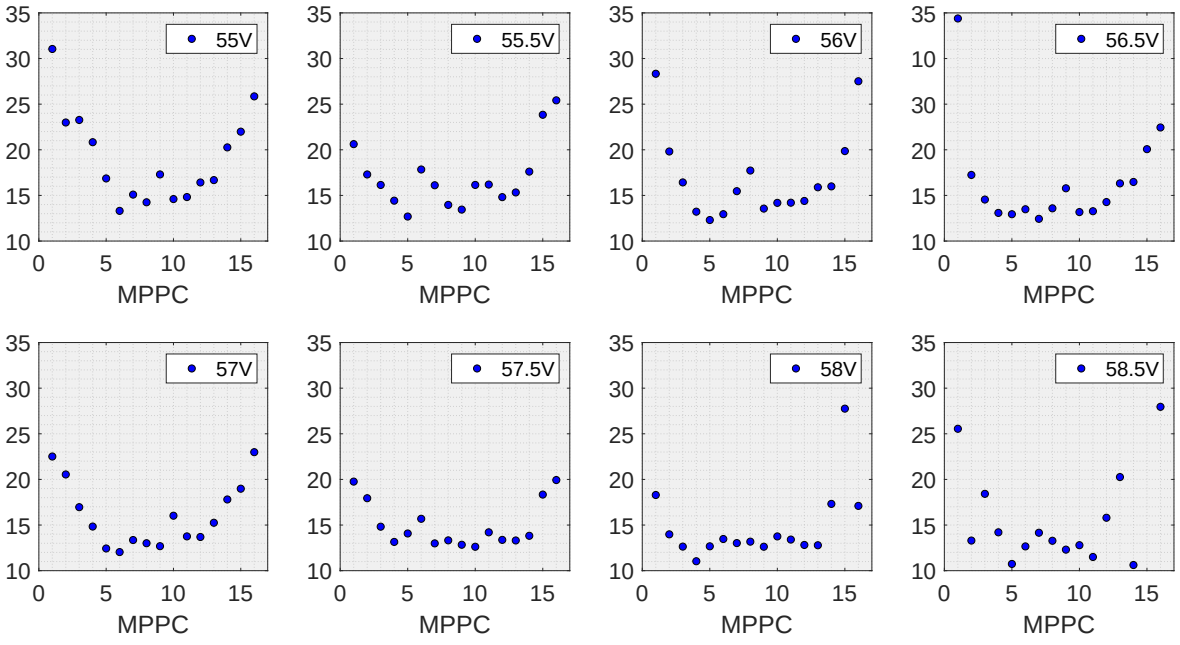

Figure 4.6: Energy resolution(%) for a resistive chain of 80 Ω obtained for 16 MPPC's+LYSO. The LYSO array is defined at the figure 3.10 (a).

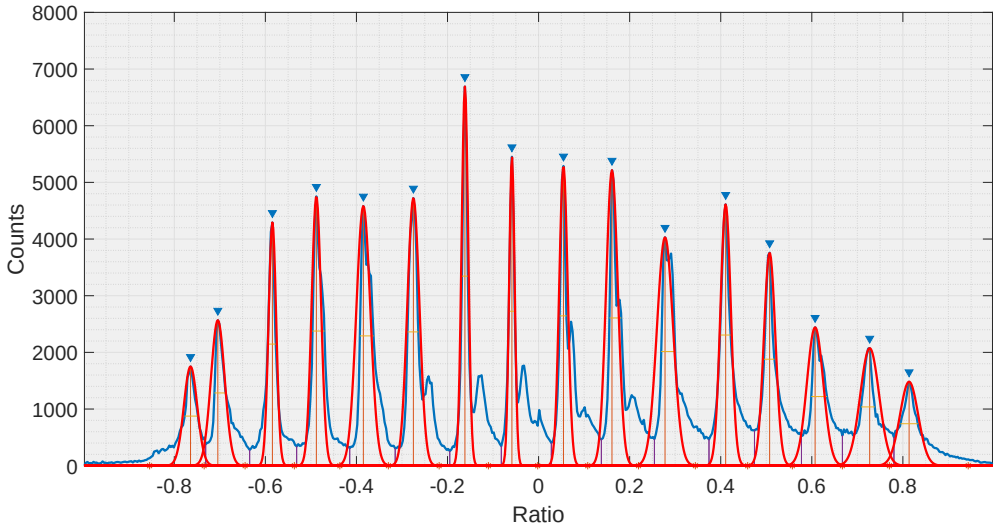

Figure 4.7: The obtained ratio spectrum for the detectors array nº2 for the V_{op} of 57,5V.

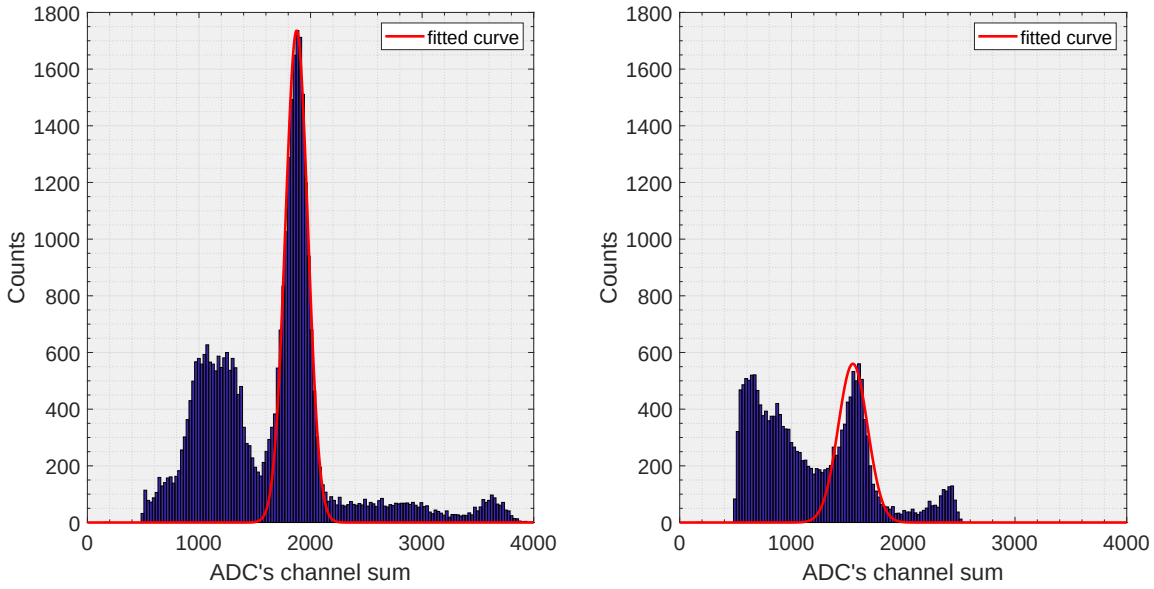

Figure 4.8: Energy spectrums obtained by the detectors nº 10 (at the left) and 16 (at the right) respectively for the V_{op} of 57.5V.

4.3 Resolution studies of the array nº3

The figure (4.11) defines the same type of spectrum as at the figures (4.3) and (4.8), but for a 40 detectors. As it was expected, with the increased number of detectors, the distance between the neighbour peaks decreases. In this case, it was necessary to use another approach

to identify all 40 peaks, and even if we could find locate almost all of them there is a clear overlaping of the neighbour peaks. This means that during the acquisition, two different crystals of the scintillator array detectors share the light photons and, consequently, the respective MPPC's produce almost the same amount of charge that in the ratio spectrum becomes more hard to distinct. As this happens throughout the array, we assumed that the upper and lower layer of crystals were not well isolated. As a result, they share between them the ammount of light, which makes some of the MPPC's to produce relatively the same ammount of charge.

Based on the obtained results, V=57 V is the optimal operational voltage for this array of detectors. The 8^{th} and the 22^{nd} peaks show the worst and the best energy resolution respectively.

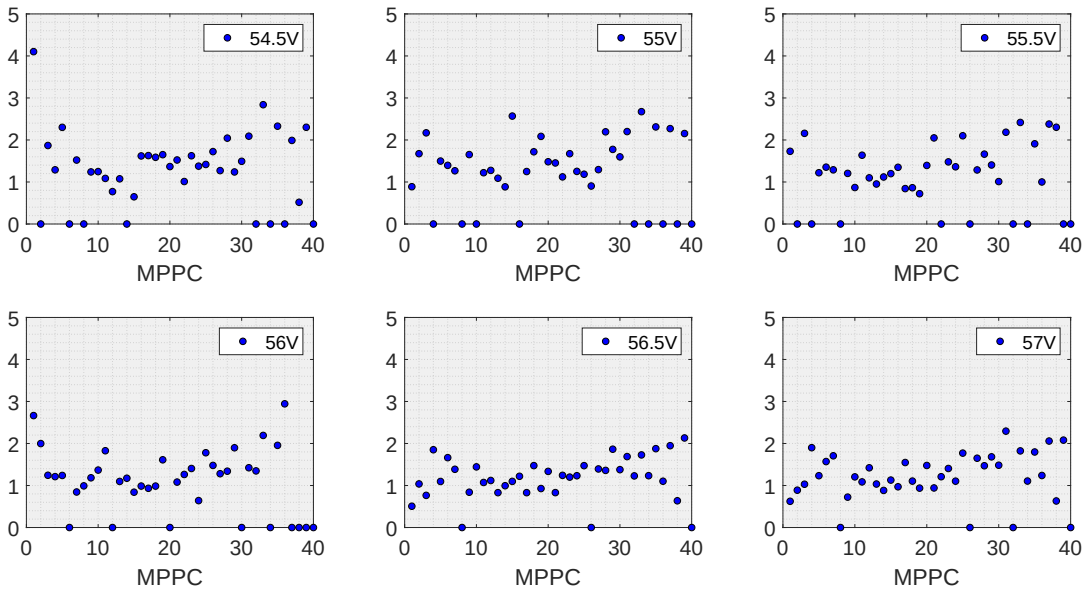

Figure 4.9: Ratio resolution(%) for a resistive chain of 205 Ω obtained for 40 MPPC's+LYSO defined at the figures ((3.9) and 3.10 (b)) respectively.

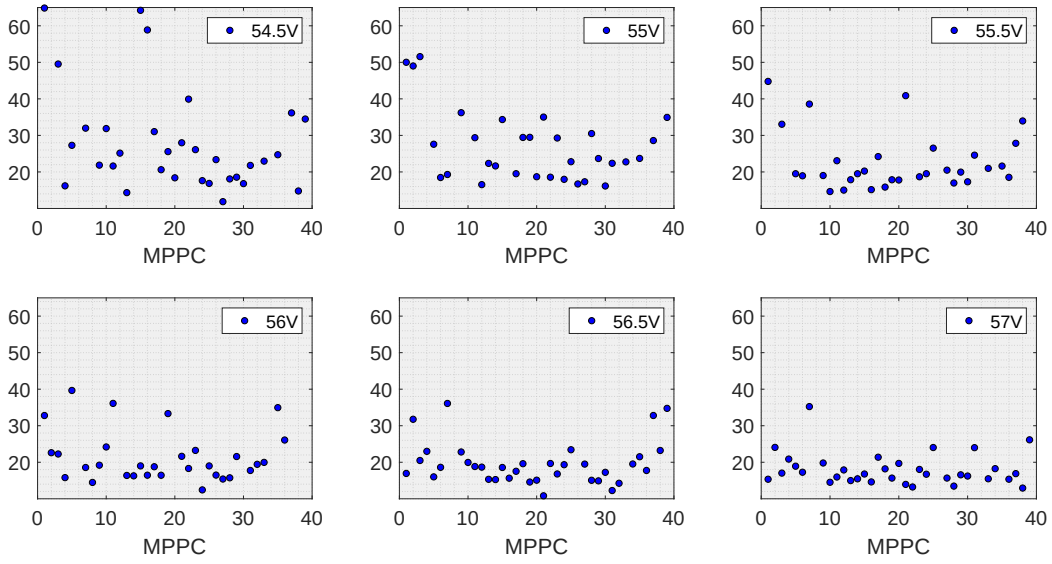

Figure 4.10: Energy resolution(%) for a resistive chain of 205 Ω obtained for 40 MPPC's+LYSO defined at the figures ((3.9) and 3.10 (b)) respectively.

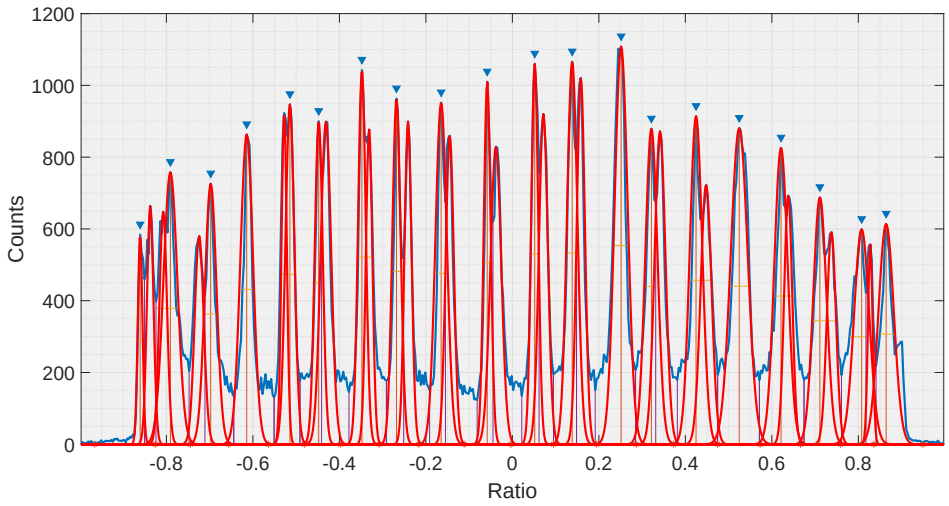

Figure 4.11: The ratio spectrum for the V_{op}=57V.

As there is a possible share of light photons and consequent overlapping of peaks in the ratio spectrum, it is possible that the energy spectrum obtained by one detector can actually have some data that, due to the share of light photons in the scintillator, was obtained by its neighbor detector. This also means that the obtained values of detectors resolution (ratio and especially energy resolution) for the array nº3 are not exact and with better isolation of scintillator crystals they could improve.

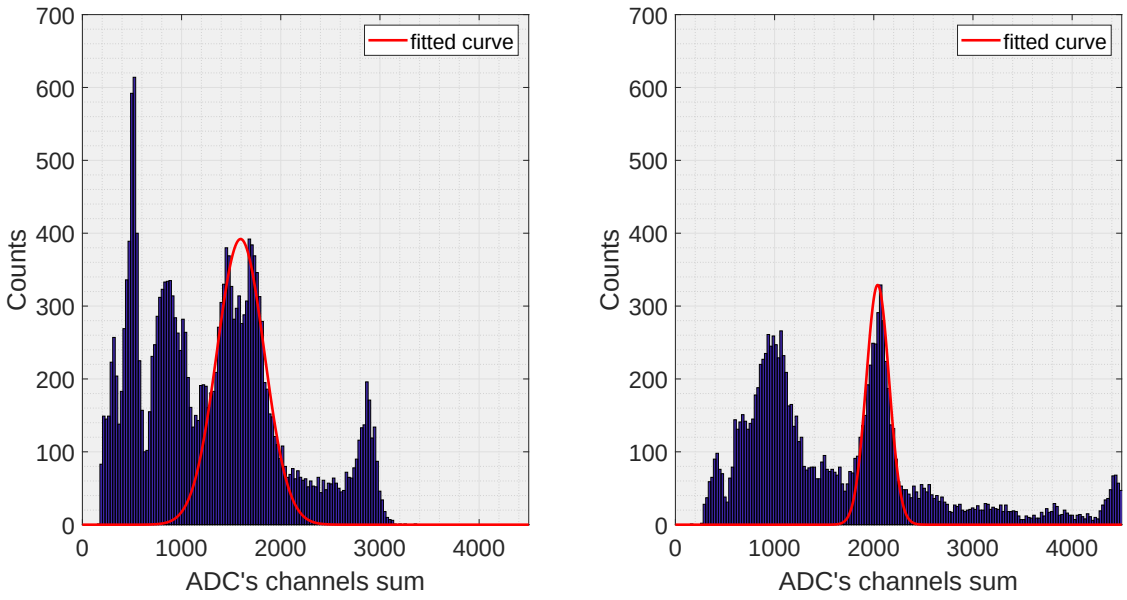

Figure 4.12: Energy spectrums detected by the 8^{th} detector (at the left) and the 22^{nd} detector (at the right).

.

Chapter 5

Conclusion

To decrease the total cost of the equipment, in this work we have studied the effect of power in the resolution of three photodetector systems (MPPC + scintillator crystal) that were connected up to the resistive chain, which allows the simultaneous reading of several MPPC coupled to an "array" of scintillating crystals. For this purpose, we studied three different electronic circuits. Each of them contains the MPPCs of the different series, that are connected with the resistive chain. Those circuits were connected to the processing circuit preamplifiers and an ADC. It was studied the effect of the operational voltage of the MPPCs on the resolution of the obtained results. For each one of the detectors, it was determined the optimal operating voltage and the ratio with the energy resolutions. The best results were obtained for the detector array nº2 for an operating voltage of 57.5 V. The obtained ratio and energy resolution for this array equals to $1.5 \pm 1\%$ and 15 ± 5 % respectively. For the detector array nº1 with $V_{op} = 74$ V, the ratio and the energy resolution values are given by 1.15 ± 0.3 % and $17.5 \pm 2\%$. Another obtained ratio and energy resolution values for a detector with $V_{op} = 57$ V array nº3 were 1.39 ± 1.1 % and $18.1 \pm 15\%$ respectively.

With these obtained results it was possible with a single resistive chain to readout the electric pulses produced by the arrays of 16 detectors. It was not possible to get the readout of the 40 detectors without pile-ups, however, this may be due to the sharing of light between the scintillating crystals of the upper layer with the lower layer. It is suggested to repeat the acquisitions in which the array of the 40 scintillating crystals but with better isolation between the crystals.

Bibliography

[1] Jadvar H. and Parker J.A. *Clinical PET and PET/CT*. Springer-Verlag, 2004.

[2] Miles N. Wernick and John N. Aarsvold. *Emission Tomography: the Fundamentals of Pet and Spect*. Elsevier Academic Press, 2004.

[3] Michael E Phelps. *Physics, Instrumentation, and Scanners*. Springer, 2006.

[4] 2018-07-08 [Online] https://www.hamamatsu.com/resources/pdf/ssd/mppc_kapd0004e.pdf, 2016.

[5] Glen F. Knoll. *Radiation Detection and Measurement*. John Wiley & Sons, Inc., 4th edition, 2010.

[6] D.L. Bailey, J.L. Humm, A. Todd-Pokropek, and A. van Aswegen, editors. *Nuclear Medicine Physics*. IAEA Library, 2014.

[7] Saha Gopal B. *Physics and Radiobiology of Nuclear Medicine*. Springer, 3 edition, 2006.

[8] BGO, LYSO and GSO - Crystal Scintillators by Omega Piezo Technology, Inc.

[9] Syed Naeem Ahmed. *Physics and Engineering of Radiation Detection*. Academic Press, 1 edition, 2015.

[10] W Chewpraditkul, L Swiderski, M Moszynski, T Szczesniak, A Syntfeld-Kazuch, C Wanarak, and P Limsuwan. Scintillation Properties of LuAG:Ce, YAG:Ce and LYSO:Ce Crystals for Gamma-Ray Detection. *IEEE TRANSACTIONS ON NUCLEAR SCIENCE*, 56(6), 2009.

[11] Maurizio Conti and Lars Eriksson. Physics of pure and non-pure positron emitters for PET: a review and a discussion. *EJNMMI physics*, 3(1):8, dec 2016.

[12] Marie Cantone and Hoeschen Christoph, editors. *Radiation Physics for Nuclear Medicine*. Springer, 2011.

[13] Didier Le Bars. Fluorine-18 and medical imaging: Radiopharmaceuticals for positron emission tomography. *Journal of Fluorine Chemistry*, 127(11):1488–1493, nov 2006.

[14] Russ Kuker, Manuel Sztejnberg, and Seza Gulec. I-124 Imaging and Dosimetry. *Molecular imaging and radionuclide therapy*, 26(Suppl 1):66–73, 2017.

[15] Jorge A Carrasquillo, Joseph A O, Volkan Beylergil, Shutian Ruan, Neeta Pandit-Taskar, Steven M Larson, Peter M Smith-Jones, Serge K Lyashchenko, Norihisa Ohishi, Toshihiko Ohtomo, and Ghassan K Abou-Alfa. I-124 codrituzumab imaging and biodistribution in patients with hepatocellular carcinoma. *EJNMMI research*, 2018.

[16] Peter E. Valk, Dominique Delbeke, Dale L. Bailey, David W. Townsend, and Michael N. Maisey, editors. *Positron Emisson Tomography, Clinical Practice*. Springer-Verlag, 2006.

[17] V. Arosio, M. Caccia, I.F. Castro, P.M.M. Correia, C. Mattone, L.M. Moutinho, R. Santoro, A.L.M. Silva, and J.F.C.A. Veloso. easyPET: a novel concept for an affordable tomographic system. *Nuclear Instruments and Methods in Physics Research Section A: Accelerators, Spectrometers, Detectors and Associated Equipment*, 845:644–647, feb 2017.

[18] R. Yao, R. Lecomte, and E. S. Crawford. Small-Animal PET: What Is It, and Why Do We Need It? *Journal of Nuclear Medicine Technology*, 40(3):157–165, 2012.

[19] M. Carles, Ch.W. Lerche, F. Sánchez, A. Orero, L. Moliner, A. Soriano, and J.M. Benlloch. Performance of a DOI-encoding small animal PET system with monolithic scintillators. *Nuclear Instruments and Methods in Physics Research Section A: Accelerators, Spectrometers, Detectors and Associated Equipment*, 695:317–321, 2012.

[20] Z Gu, D L Prout, R W Silverman, H Herman, A Dooraghi, and A F Chatziioannou. A DOI Detector With Crystal Scatter Identification Capability for High Sensitivity and High Spatial Resolution PET Imaging. *IEEE transactions on nuclear science*, 62(3):740–747, jun 2015.

[21] H Uchida, T Sakai, H Yamauchi, K Hakamata, K Shimizu, and T Yamashita. A novel single-ended readout depth-of-interaction PET detector fabricated using sub-surface laser engraving. *Physics in Medicine and Biology*, 61(18):6635–6650, sep 2016.

[22] Paul Lecoq. Development of new scintillators for medical applications. *Nuclear Instruments and Methods in Physics Research Section A: Accelerators, Spectrometers, Detectors and Associated Equipment*, 809:130–139, feb 2016.

[23] K Ghassemi, A Sato, K Kobayashi. 2018-11-26 [Online] https://www.hamamatsu.com/resources/pdf/ ssd/mppc_kapd9005e.pdf Technical note MPPC (HAMAMATSU), 2017.

[24] S10362-11 series MPPC ® (multi-pixel photon counter) New type of Si photon-counting device, Active area: 1×1 mm.

[25] S13360 series - MPPCs for precision measurement MPPC ® (Multi-Pixel Photon Counter).

[26] MPPC ® arrays S13615 series.